Engineering Applications of Computational Fluid Mechanics Vol. 8, No. 4, pp. 477–487 (2014)

NUMERICAL MODELLING OF PLUNGE POOL SCOUR EVOLUTION IN NON-COHESIVE SEDIMENTS

Gaël Epely-Chauvin, Giovanni De Cesare* and Sebastian Schwindt

Laboratory of Hydraulic Constructions, School of Architecture, Civil and Environmental Engineering, Ecole Polytechnique Fédérale de Lausanne, EPFL-ENAC-LCH, Station 18, CH-1015 Lausanne, Switzerland

** E-Mail: giovanni.decesare@epfl.ch (Corresponding Author)*

ABSTRACT: Turbulences in liquids caused by jets can be of interest for numerous applications. For one, it concerns flood spillway structures within civil engineering but also is key in any area where turbulent mixing is present. The numerical simulations of jets that impinge into plunge pools are still in an early phase of their development. This paper verifies the accuracy of the Flow-3D software package in regards to simulating 3D scouring processes generated by turbulent water jets impinging on a sediment bed. Scour calculations are performed based on previously examined laboratory experiments. The results of the numerical model compare well with the experimental results in terms of the scour depth and the ridge height which accumulates downstream of the scour hole. The impact angle of the jet is identified as a driving parameter for the establishment of steady state conditions of scour depth and ridge height.

Keywords: Flow-3D, impinging jets, scour, plunge pool, turbulent mixing

1. INTRODUCTION

The prediction of local scour depths which develop downstream of hydraulic structures plays an important role in their design. Excessive local scour may progressively undermine the structure's foundation. However, as complete protection against scour is difficult to realize in terms of costs, the maximum scour depth and upstream slope of the scour hole are intended to be predictable to minimize the failure risk (Gisonni and Hager, 2008).

The scour created by water jets impinging on a plunge pool has been subject of numerous experimental and numerical studies. It is a complex phenomenon involving three phases: water, air and rock or sediment bottom (Bollaert and Schleiss, 2005). The first studies on jet scour were conducted by Schoklitsch (1932) and Veronese (1937) followed by Rouse (1940) and Laursen (1952). Two examples of efforts to create numerical simulations regarding suspended materials are the studies of the Pearl River estuary by Chau and Jiang (2001, 2004).

Bollaert and Schleiss (2005) and Manso et al. (2009) experimentally assessed transient pressures inside closed-end fissures on the rock bottom of a plunge pool impacted by high-velocity water jets and developed models for joint break - up. More recently, Federspiel (2011) studied dynamic pressures encompassing a block and developed a method for the description of block ejection. The influence of jet air entrainment was investigated by Canepa and Hager (2003) for movable bed and by Duarte et al. (2012) for rock foundations.

The significant increase of computational performance enabled the rise of numerical solutions for simulating scouring processes, e.g. Zhao and Fernando (2007) used the ANSYS software *Fluent* to simulate scouring near offshore pipes and Kitamura and Wang (2001) simulated the scour process in a plunge pool for loose bed material.

Scouring processes are analyzed not only to minimize their negative effects, but also for industrial purposes. Here, mixing processes, recently analyzed by Hunter et al. (2013) and sediment entrainment, investigated by Jenzer Althaus et al. (2011), might be of interest.

The availability of numerous data from laboratory experiments enables the validation of numerical simulations. The purpose of this paper is to verify the effectiveness of the numeric routine incorporated in the Flow-3D package for jet-induced scour processes. Flow-3D has already been successfully applied for analysis of hydraulic and sediment transport problems. For instance, Ozmen-Cagatay and Kocaman (2011) used Flow-3D for simulating a dam-break where the implemented turbulence model showed good results related to laboratory experiments.

Received: 25 Nov. 2013; Revised: 30 Apr. 2014; Accepted: 24 Jun. 2014

In this paper, the Flow-3D software is validated in terms of its capabilities for predicting jet induced scour processes. In addition, the driving parameters for steady-state conditions are investigated. The validation is based on the simulation of the experimental setup built by Pagliara et al. (2008b). The occurring scour holes and the ridges downstream of the latter are compared with available experimental results. The general validity of the numerical model for erosion processes has already been shown by De Cesare et al. (2011) for a scaled model (1:65) of the Koman dam plunge pool (Albania).

2. SCOUR BY FALLING JET

The general process of scouring process in loose and non-cohesive sediments is sketched in Fig. 1. An impinging jet of diameter D_i impacts the free surface with an angle θ_i and a velocity v_i. The jet core (i.e. the zone where the velocity of impinging water is in the extent of v_i) immediately starts to diffuse linearly with an angle θ_s in the tail water; y_k denotes the core length. The applied values are presented later in the text. Aiming at the identification of driving parameters besides the air entrainment of jets, the phenomenon is reduced to a single phase jet without air entrainment. The nature of the resulting velocity field is Gaussian (Bin, 1993) but the velocities with air entrainment were found to be more important (Duarte et al., 2014). Therefore, the observed results may be amplified in prototypes. The parameters z_m and z_M denote the scour hole depth and ridge height, respectively.

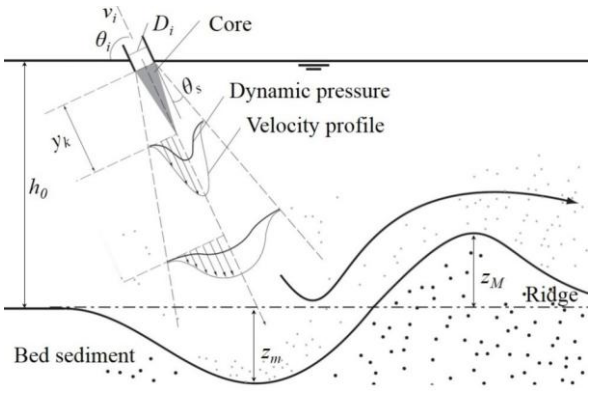

Fig. 1 Scour hole with classic geometry and process and experimental setup characteristics of Pagliara et al. (2006) for a submerged jet.

The diffusion cone then impacts the sediment bed and the scour process starts. The jet reaches the water in the plunge pool at high velocity, diffuses and impacts the initially flat erodible bed. The jet induced flow velocity is still sufficient to uplift and to transport bed material downstream at high rate. Thus, for a short duration, the scour hole develops faster in its vertical dimensions than in its horizontal ones. As the scour hole gradually enlarges in time, the water depth h_0 (bed level to fluid surface) increases and so the flow cross-section. Considering the conservation of mass, the mean flow velocity reduces accordingly and therefore, also the sediment transport capacity of the flow decreases in the scour hole logarithmically in time. Finally, after a certain time, the bed velocity reduces to an extent that prevents any further sediment erosion in the scour hole.

3. NUMERICAL MODEL

3.1 Description of governing equations

The software Flow-3D (Flow Science Inc., 2009) is used in this study. It is a CFD package combining pre and post processing tools. Equations are formulated by area and volume porosity functions: zero porosity regions define obstacles and area porosities may define thin porous baffles. The Navier-Stokes equations are used to describe fluid velocities. Equations used to express the sediment model behaviour are based on the Flow-3D manual (Flow Science Inc., 2011) and Brethour (2003). All terms which are not further necessary for comprehension, are omitted in the following paragraphs.

3.1.1 Sediment suspension model in general

The Flow-3D model aims to describe the three dimensional behaviour of packed and suspended sediments. The latter are caused by erosion of the former. The suspended sediment advects and drifts with the fluid driven by the local pressure gradient. The motions are governed by a "drifting" submodel.

Packed sediment does not move as it is bounded by adjacent sediment particles. In such regions, fluid flow stops and permeability is set to zero. At the interface between fluid and packed sediment, the latter can be eroded and entrained into suspended sediment. The interface shape is governed by a "lifting" submodel, which is enabled when the shear stress exceeds a critical value.

The solid-like behaviour of sediments is implemented by applying a drag model. After sedimentation, a region is considered as packed

(i.e. solid) when the concentration exceeds the "critical solid fraction", $f_{s,cr}$. Therefore, the drag in such a region is infinite.

3.1.2 Equations for viscosity and density evaluation

Both, the viscosity and density change in terms of the sediment concentration. The solid volume fraction, f_s, is the ratio of volume occupied by sediment and the total volume, i.e. the sum of suspended and packed sediment concentration is divided by the density of the sediment, ρ_s. The liquid fraction, f_l, is the fraction of the volume occupied by liquid and the total volume, so that

$$f_l + f_s = 1. \quad (1)$$

Viscosity is increasing with increasing suspended sediment fraction. When the cohesive solid fraction, $f_{s,co}$, and the solid volume fraction are equal, particles interact and cause solid-like behaviour. This phenomenon is implemented in the momentum equation (4) in terms of a linear drag constituent. Concerning viscosity, its average value of the mixture, μ^*, is derived by:

$$\mu^* = \mu_f\left(1 - \min(f_s, f_{s,co})/f_{s,cr}\right) \quad (2)$$

where μ_f denotes the molecular viscosity of the liquid and $f_{s,cr}$ the critical solid fraction. If the solid fraction exceeds $f_{s,cr}$, sediment particles are considered as being packed. In this case, the flow abates due to the drag coefficient K which becomes infinite. Therefore, also K is computed in function of the solid volume fraction as below shown.

$$\mathrm{K} = \begin{cases} 0 & if \quad f_s < f_{s,co} \\ K_f & if \ f_{s,co} < f_s < f_{s,cr} \\ \infty & if \quad f_{s,cr} < f_s \end{cases} \quad (3)$$

where

$$K_f = [(f_{s,cr} - f_{s,co})/(f_{s,cr} - f_s)][(f_{s,cr} - f_{s,co})/(f_{s,cr} - f_s)\text{-}1]$$

Thus, in order to model loose and non-cohesive sediment, $f_{s,cr}$ and $f_{s,co}$ have to be defined very closely. Finally, K is introduced to the momentum equation:

$$\partial \boldsymbol{u}/\partial t + \boldsymbol{u} \cdot \nabla \boldsymbol{u} = -\nabla P + \nabla \cdot \tau + g - K\boldsymbol{u} \quad (4)$$

where $\boldsymbol{u}$ describes the fluid velocity vector, P denotes pressure and τ shear stresses; g accounts for body forces. Thus, the left hand side describes the local and convective acceleration terms, while the right hand side stands for shear resistance.
The density of the suspension, ρ', therefore is a linear function of the sediment fraction:

$$\rho' = \rho_l + f_s(\rho_s - \rho_l) \quad (5)$$

where ρ_S is the density of the sediment and ρ_l of the liquid phase (water). The settling component of the model presumes the sediment particles to be spherical and their velocity to be small. Thus, viscous effects dominate in the flow encompassing each sediment particle.

3.1.3 Description of "drifting" submodel (suspended particles)

The settling (i.e. drift) coefficient is defined as:

$$D_f = d^2(\rho_s - \rho_l)/18\mu_f \quad (6)$$

The drift velocity is determined as:

$$\boldsymbol{u}_{drift} = D_f f_l \nabla P/\rho' = f_l d^2 \nabla P(\rho_s - \rho_l)/(18\mu_f \rho') \quad (7)$$

where d denotes the mean diameter of the sediment particles and μ_f the liquid viscosity. $\nabla P/\rho'$ describes the body acceleration. The liquid fraction f_l is implemented to account for the presence of a fluid (here: water). Thus, $\boldsymbol{u}_{drift} = 0$ in regions of solid-like behaving packed sediments.

3.1.4 Description of "lifting" submodel (packed bed)

At interfaces, the shear stress causes erosion of sediment. The amount of eroded sediment depends on the shear stress with its critical value, as well as the densities of the solid and the fluid. The critical Shields parameter is used for defining incipient of sediment motion. The dimensionless critical shear stress has to be exceeded for lifting a characteristic sediment particle. It is computed as:

$$\Theta_{crit} = \tau_{crit} / [g \cdot d \cdot (\rho_s - \rho_l)] \quad (8)$$

where τ_{crit} denotes the critical effective shear stress at the bed level for sediment transport inception. In order to account for a threshold value for the incipient of sediment motion, the shear velocity $u_{0*} = \sqrt{\tau/\rho'}$ is introduced. It is used for estimating the lift rate of sediment from the packed bed by the excess shear velocity: $\sqrt{(\tau - \tau_{crit})/\rho'}$. Introducing this into the formula of the lift velocity results in:

$$\boldsymbol{u}_{lift} = \alpha \boldsymbol{n}_s \sqrt{(\tau - \tau_{crit})/\rho'} \quad (9)$$

where $\boldsymbol{n}_s$ denotes the normal vector at the sediment bed - water interface. α is the (dimensionless) probability of a particle being lifted from the packed bed which normally is inferior to or equals unity. The "lifting" process

behaviour is also influenced by the angle of repose that accounts for the slope stability supported by the packed sediment, e.g. sediment with a small angle of repose is prone to be instable. In the model discussed here, the angle of repose ς is a parameter in degrees entered by the user. The actual angle of the surface φ results from the dot product of the normal vector of the packed sediment interface and the gravity vector $\boldsymbol{g}$:

$$\varphi = \boldsymbol{n}_s \cdot \boldsymbol{g} \,/\, |\boldsymbol{g}| \tag{10}$$

The effective critical shear stress is computed based on the critical shear stress acting on a horizontal plane, where $\varphi = 0$. Accounting for the slope and the angle of repose, the effective critical shear stress is derived by (Lane, 1955):

$$\tau_{crit} = \tau_{0,crit}\sqrt{1 - sin^2\,\varphi / sin^2\,\varsigma} \tag{11}$$

The square root and therefore also τ_{crit} in eq. (11) are zero when the angle of repose equals the surface slope. Thus, any gravity driven flow action erodes the sediments. When the surface slope φ is larger than ς, eq. (11) is omitted and erosion takes place even if there is no fluid motion.

In a nutshell, sediment motion results from resolving the advection-diffusion equation and implementing drift and lift forces.

3.2 Validation of numerical model

As already mentioned, the focus of this paper is the verification of the effectiveness of the numerical methods included in Flow-3D for computing sediment scour. For this purpose, scour profiles and evolution measurements carried out by Pagliara et al. (2008b), were used as benchmarks.

3.2.1 Experimental setup of Pagliara et al. (2008b)

The experiments made by Pagliara et al. (2008b) investigated the temporal development of plunge pool scour. The explicit data results were maximum scour hole depth, maximum ridge height and spatial development evolution. Accounting for simulation duration, four tests among the 54 conducted were chosen to validate the sediment model. In order to be able to compare and validate the results representatively for all configurations, the sampling was made by means of different experiment configurations varying the jet impact angle θ_i, the discharge and the densimetric particles Froude number, where the latter one is denoted by $F_{d90} = u/(g'd_{90})^{1/2}$ with the reduced gravitational acceleration $g'=[(\rho_s-\rho_l)/\rho_l]g$. This definition of Froude number combines the jet flow behaviour with sediment characteristics.

The experimental setup is shown in the sketch of Fig. 1. Tests involved nearly uniform sediment with a median diameter d_{50} = 0.00115m and d_{90} = 0.00135 m. Where the sediment non-uniformity parameter $\sigma = (d_{84}/d_{16})^{1/2}$ = 1.15, the density of the particles ρ_s = 1400kg/m^3 and the angle of repose was set to ς = 35.

The rectangular shaped channel is 0.70m deep and 0.50m wide. The sediment layer was set to a thickness of 0.30m. The flow depth h_0 is kept so that the tail water ratio varies between $0.80 \leq h_0/D \leq 10$. The tests characteristics are summarized in Table 1, where parameter Q denotes the jet volume flow rate and $T = t\cdot(g'd_{90})^{1/2}$ denotes the dimensionless time.

Table 1 Parameters of experimental test selected to benchmark the numerical model.

Test #	θ_i [°]	Q [l/s]	D_i [m]	T [-]	F_{d90} [-]	d_{50} [m]	σ [-]
Test 1	45	1.5	0.035	7.2	27.8	0.00115	1.15
Test 2	60	1.5	0.035	5.1	27.8	0.00115	1.15
Test 3	45	3.5	0.0217	5.9	25	0.00115	1.15
Test 4	30	2.1	0.0217	11.9	39	0.00115	1.15

3.2.2 Computational field: mesh characteristics

To model the experimental setup, a Cartesian coordinate system with a 3D orthogonal grid constituted by 10^6 cells is used. Different types of mesh resolution have been tested, where this offers best precision/computation time results. The mesh resolution is finally determined as an optimum of computation time and the proper reproduction of the relevant hydraulic phenomenon, i.e., a minimum number of 5 cells is necessary for the simulation of the jet (Gabl et al., 2014). Boundaries are defined as follows: "constant tail water" at inflow (y_{min}) and outflow (y_{max}). "Wall" at x_{max} and z_{min}, "free surface" at z_{max} and x_{min} is defined as a symmetry plane like indicated in Fig. 2.

The mesh aspect ratio is maintained at [1:1:1]. The numerical model dimensions are:

x: 0.5 m; y: 1.9 m; z: 0.65 m.

The resulting cell dimensions are [0.9 cm: 0.8 cm: 0.85 cm]. Another reason for the choice of this rectangular mesh is the numeric stability, where

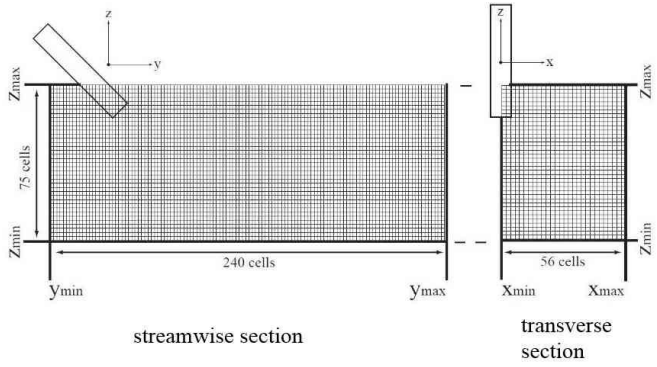

Fig. 2 Physical grid arrangement: dimensions and characteristics.

the adjacent cell size ratio, i.e. the aspect ratio, equals unity.
The $k-\varepsilon$ model is used as turbulence closure model. During the calculations, continuous monitoring of all major hydrodynamic and sediment parameters is performed.

3.2.3 Computation time

The laboratory experiments by Pagliara et al. (2006) lasted until "the scour hole undergoes practically no more changes". This complies with test durations up to 53 x 10^3*s* (Pagliara et al., 2008b). Due to the limits of computational power and data storage capacity, the end time was chosen in terms of hydraulic stability, where the erosion process may still go on, but gently. For test 1, a sample simulation has been run over 180*s* for comparing the average mean kinetic energy (hydraulic stability) with the packed sediment mass (mass stability) in the model. Hydraulic stability can be claimed to be achieved after about 30*s*, where sediment is still eroded, even at the end of the prolonged simulation duration. This complies with the expectations of the time scale of flow responses being much smaller than the one of the bed form evolution (McLean et al., 1994).
Considering that the computation takes up to two thousand times longer than the experiments duration, the end time for each configuration was set to 120*s* (up to 72*h* computation time).

3.2.4 Implementation in Flow-3D

The channel is introduced applying symmetry principles in order to reduce the computational efforts. A baffle in the jet is set up for controlling the jet discharges. The sediment is implemented by an own component of type "packed sediment". Its angle of repose is, in line with Pagliara et al. (2008a), set to $\varsigma = 35°$ using the sediment scour in physics tab. The principle is illustrated in Fig. 3, where the boundary conditions of simplified model are indicated. Where W indicates a "wall" boundary, i.e. a wall adhesion defined by surface tension, which is defined by the SIGMA coefficient. The flow rate boundary is located on the top surface, open only at the impinging jet entry. *S* is the symmetry condition which means that flow velocity derivatives are zero. The pressure condition *P* simulates ambient conditions at the corresponding surface, i.e. in this case the laboratory model environment. (Flow Science Inc., 2011)

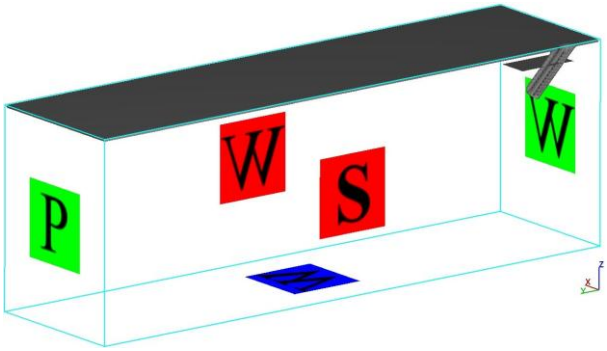

Fig. 3 Geometry and boundary conditions of simplified model.

3.2.5 Hardware issues

The program (Flow-3D) is run on a Windows 7 Enterprise operating system (64 - Bit, Service Pack 1). The machine has 16 Xenon cores (E5630@2.53 GHz) and 24GB of installed memory (RAM) at its disposal. The overall CPU time of the simulations is in average about 1.86 x 10^5*s* which complies with 1.5 x $\cdot 10^3$*s* per CPU.

3.3 Results of simulation

3.3.1 Scour depth and ridge height

Here, the Flow-3D results are compared with the selected experimental benchmarks results. Fig. 5 shows the scour profile at different time steps for test 1. Scaled velocity profiles are indicated which also visualize the diffusion cone mentioned earlier (Fig. 1). The general shape of the scour hole profile is in good agreement with the classical scour shape like shown in Fig. 1. This can be reproduced in the three-dimensional illustration of the final time step shown in Fig. 4. The further analysis of the results is examined in the 2D plane (y-z).

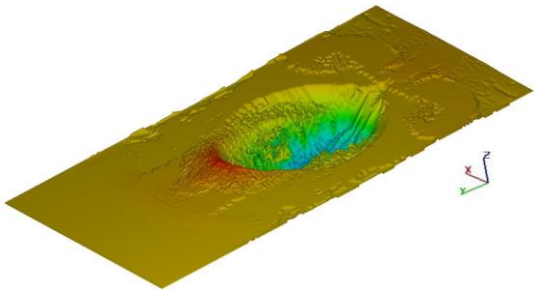

Fig. 4 Qualitative 3D plot of packed sediment height after 120 seconds (flow in y-direction).

The dimensionless scour hole depth, $Z_m = z_m/D$, and the dimensionless ridge height, $Z_M = z_M/D$, are plotted versus the non-dimensional time T in semi-logarithmic scale for each numerical test in Fig. 6. Also the experimental results (Pagliara et al., 2008b) are indicated. The figure shows that the Flow-3D sediment model provides good overall agreement with experiments for the simulated time period. Both tendencies and values provide good estimates of experimental results.

3.3.2 Scour shape

A recent publication of the already mentioned Koman Dam in Albania in De Cesare et al. (2011) is based on an extended version of the here presented numerical model. This model proves the accuracy of the shape of the scour hole. The detailed discussion is included in the earlier mentioned article of De Cesare et al. (2011). For completeness, the results are briefly reproduced here. First, the underlying laboratory experiments are compared with the prototype shown in Fig.7.
Fig. 8 shows the velocity vectors on the background of the volume fraction of packed sediments. Only the final situation at t = 120s is shown here, as the flow pattern does not change throughout the simulation. The counter clockwise vortex in the y–z plane illustrates well the development of the scour hole. The jet-induced accelerated stream hits the ground, erodes the sediments and transports the latter partially downstream.
A significant part of the sediment accumulates at the end of the scour hole, where the stream splits between the counter clockwise turning vortex part and the normal downstream flow. Due to this split, the flow velocity drops, consequently, the transport capacity decreases and the ridge forms.

4. DISCUSSION

The numerical simulation is generally restricted by computation power and the simplifications

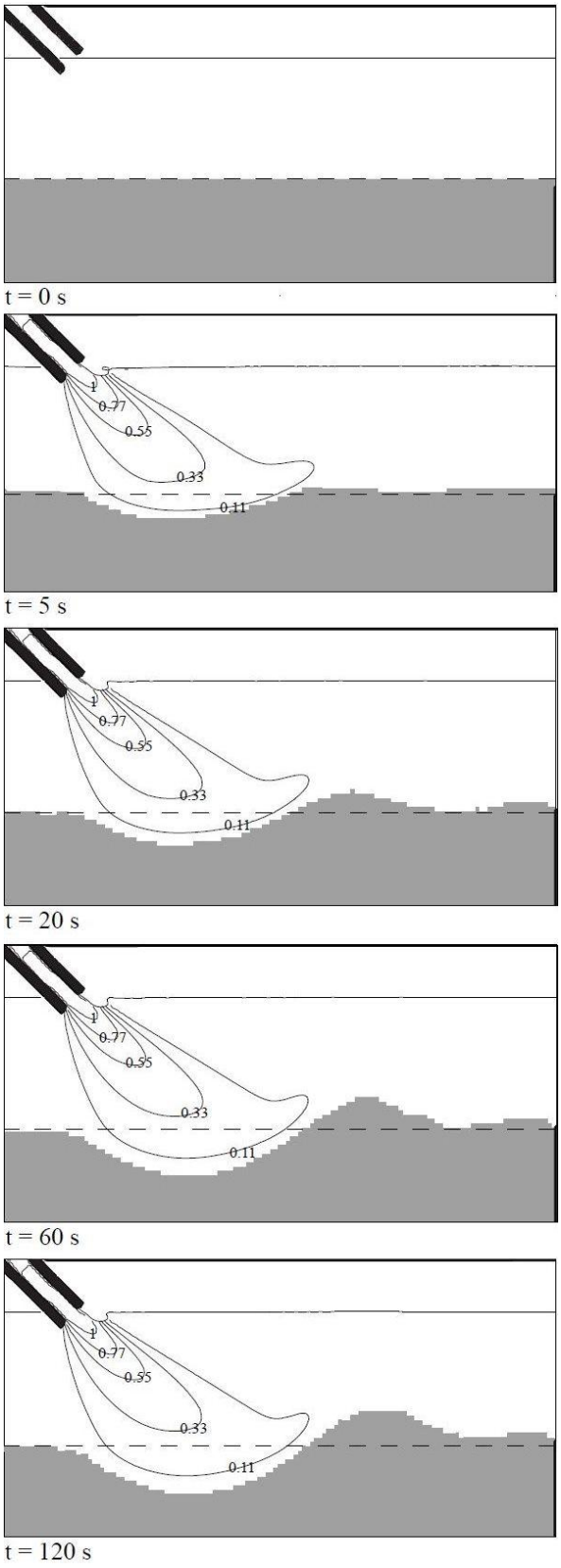

Fig. 5 Test 1 with F_{d90} =27.8, θ_i = 45° in a sequence of profiles from t = 0s to 120s; after initiating the jet (20s), the scour hole and the ridge are developing until reaching a state which only changes in minor orders after 60s and finishing in nearly hydraulic and sediment steady-state conditions at 120s.

which inevitably come up. Thus, the end of the calculation does not exactly comply with the end time of the laboratory experiments and generally excerpts can be contemplated for the analysis of correlations. Important is the identification of the moment when the steady state of the scour phenomena (ridge height and scour depth) is reached. This issue can be observed especially in Figs. 6 I(a) and I(d) for the ridge height and in Figs. 6 II(a) and II(b) for the scour hole depth. The flattening of the curves indicates the reach of the steady state. Whenever steady state occurred

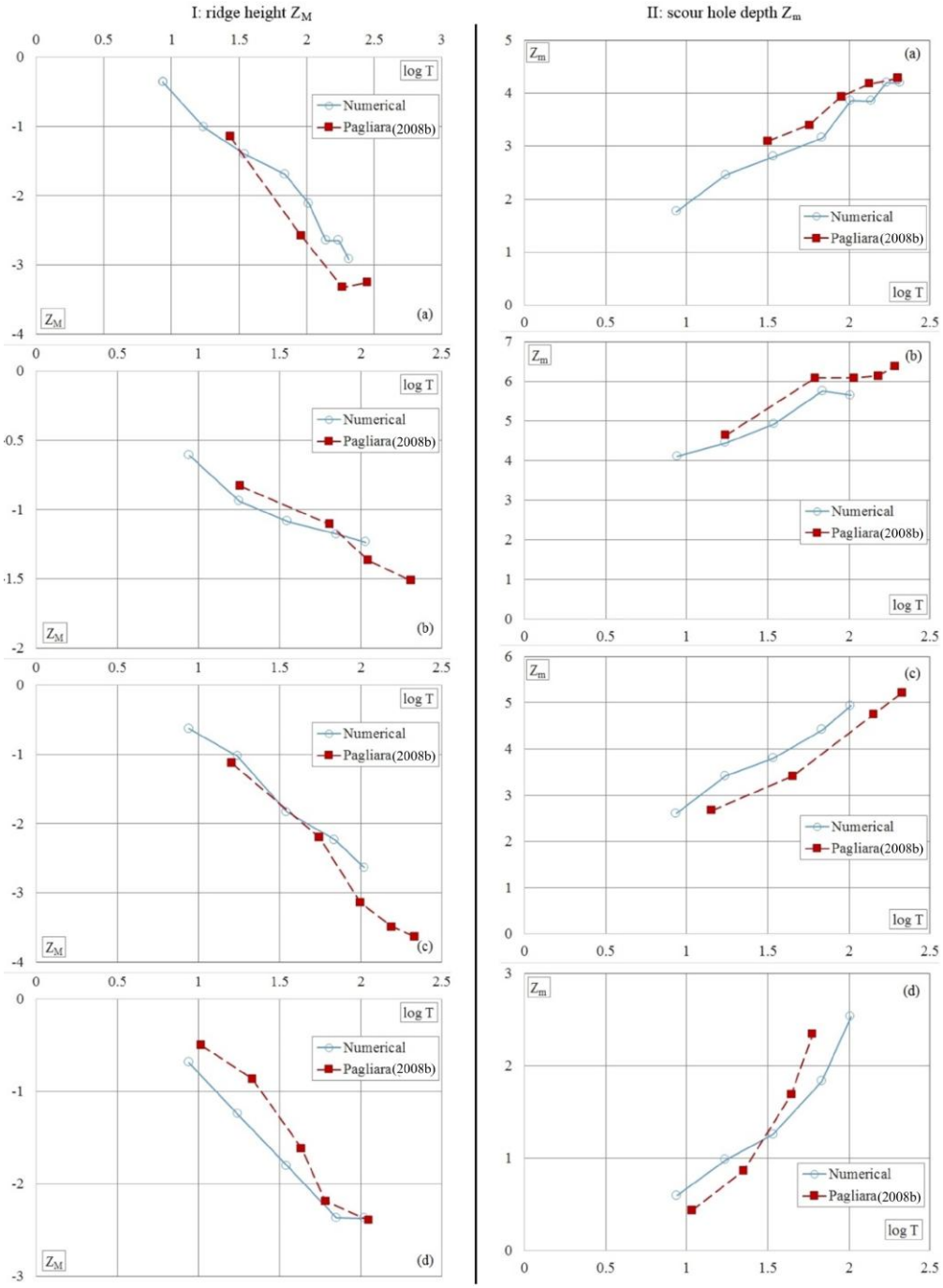

Fig. 6 Comparison of numerically and experimentally derived dimensionless (I) ridge height Z_M and (II) scour hole depth Z_m(log T) for: (a)-Test 1 [θ_1 = 45, Q = 1.5 l/s], (b)-Test 2 [θ_2 = 60°, Q = 1.5 l/s], (c)-Test 3 [θ_3 = 45, Q = 3.5 l/s], (d)-Test 4 [θ_4 = 30°, Q = 2.1 l/s].

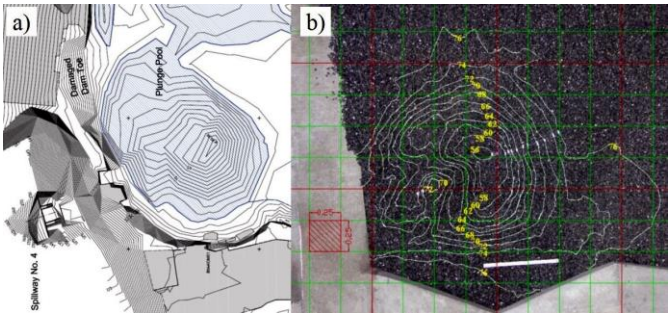

Fig. 7 Scour hole shape a) in Koman dam prototype and b) in laboratory model based on De Cesare et al. (2011).

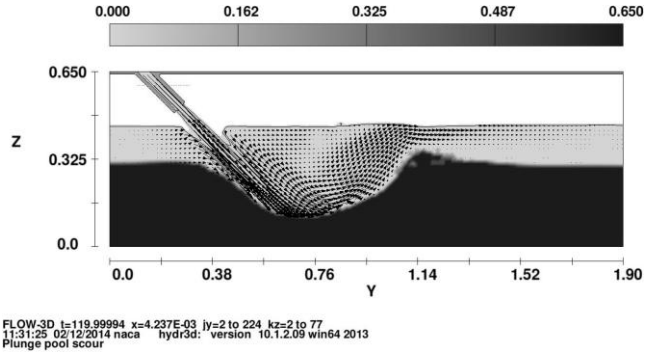

Fig. 8 Volume fraction of packed sediments with plain velocity vectors at t = 120 s (maximum flow velocity $\mathbf{u}_{max} \approx 5$ m/s).

in the laboratory experiments, the numeric computations show the same time evolution, i.e. a constant ridge height, resp. scour depth. The same holds for the experiments conducted by Pagliara et al. (2008a) which can be understood as an expansion in 3D from 2D of the experiments by Pagliara et al. (2006).

The numerically and experimentally derived values for the dimensionless scour hole depth Z_m and ridge height Z_M are compared in Figs. 9 and 10 for distinct points in time, e.g. the numerical value and the experimentally value are compared after 10 minutes of simulation and experiments, respectively. The coefficient of determination, R^2, is obtained by opposing the derived laboratory and numerical data series. For the dimensionless ridge height, R^2_{ZM} = 0.898 and for the dimensionless scour hole depth, R^2_{Zm} = 0.932. Recalling that $R^2 = 1$ means perfect agreement of the compared data sets, the obtained values for the coefficient of determination concerning the scour depth and the ridge height indicate high concordance between the results of the numerical simulations and the laboratory experiments (Hartung et al., 2005).

The outcomes concerning the impact angle can be summarized in line with these from Pagliara et al. (2006 and 2008b). The steeper the impact angle θ_i, the sooner is the steady state of the scour depth attained and the longer takes the reach of a steady state of the ridge height. Vice versa, for smaller values of the impact angle θ_i, the steady state of the ridge height is reached sooner and the establishment of the steady state of the scour depth takes longer. In agreement with the laboratory experiments, the impact angle θ_i has a major influence on the development of steady state conditions of the bed shape.

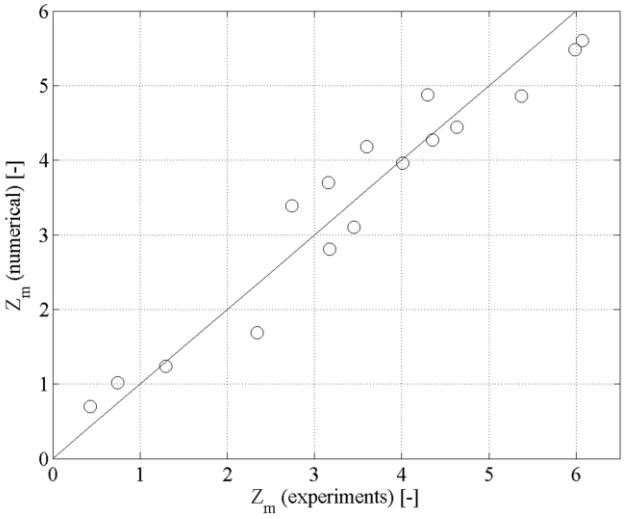

Fig. 9 Comparison of experimentally and numerically derived values for dimensionless scour depth Z_m.

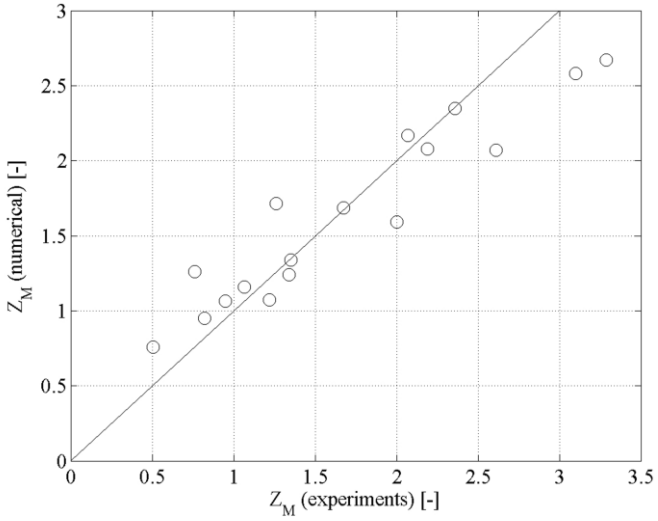

Fig. 10 Comparison of experimentally and numerically derived values for dimensionless ridge height Z_M.

5. CONCLUSIONS

The capability of the Flow-3D sediment routine has been validated by simulating existing experimental configurations and comparing the numeric results with experiment measurements. The scour process has already successfully been investigated formerly by Pagliara et al. (2006 and 2008b) in laboratory experiments and by De Cesare et al. (2011) for a case study based on both numerical and physical model tests, as well as on-site observations. The presented results show satisfactory agreement in general for measured and calculated ridge height, scour depth and spatial development. The direct comparison using the coefficient of determination R^2 indicates values of about 0.9 which confirm the good concordance between numerically and experimentally obtained results.

According to the discussion section, the numerical model results in analogical physical deductions as the laboratory experiments: the impact angle θ_i could be identified as a key parameter for the reach of steady state conditions of ridge height and scour depth.

The numerical model is a powerful tool to complement experimental analysis. However, long term simulations have to be performed to validate the model's ability to produce basic scouring analysis. Particular attention has to be paid on the mesh resolution and turbulence model characteristics that may influence the results.

Another potential perspective lies in the use of non-uniform particles with a wide grain size distribution and their influence on the armouring of the sediment bed.

ACKNOWLEDGEMENTS

The technical support from Frieder Semler (Flow-3D Germany) was very helpful. The usual further detailed acknowledgments are skipped in order to remember the principal author of this paper whose eventful life came to an abrupt end in winter 2012.

NOTATION

The following symbols, subscripts and greek letters appear in this paper.

D_f	=	drift coefficient
D_i	=	jet diameter
d	=	sediment diameter
F_{d90}	=	$u / (g' d_{90})^{1/2}$ densimetric particle Froude number
f_l	=	fluid volume fraction
f_s	=	solid volume fraction
$f_{s,co}$	=	cohesive solid fraction
$f_{s,cr}$	=	critical solid fraction
g	=	gravitational acceleration
g'	=	$[(\rho_s - \rho_l)/\rho_l]g$ reduced gravitational acceleration
h_0	=	tail water depth
K	=	drag coefficient
$\boldsymbol{n}_s$	=	bed surface normal vector
P	=	pressure
Q	=	jet volume flow rate
T	=	$t \cdot (g' d_{90})^{1/2}$ dimensionless time
t	=	time
$\boldsymbol{u}$	=	fluid velocity vector
$\boldsymbol{u}_{drift}$	=	particle drifting velocity
$\boldsymbol{u}_{lift}$	=	particle lifting velocity
u_{0*}	=	shear velocity
v_i	=	jet velocity
y_k	=	jet core length
Z_M	=	z_M/D relative ridge height
Z_m	=	z_m/D relative scour depth
z_M	=	ridge height
z_m	=	scour depth
α	=	probability that a particle is lifted from the packed surface
∇P	=	body acceleration
φ	=	actual slope angle
μ^*	=	average viscosity
μ_f	=	molecular liquid viscosity
ς	=	angle of repose
ρ'	=	mixture density
ρ_l	=	fluid density
ρ_s	=	sediment particle density
σ	=	non-uniformity parameter
τ	=	shear stress
$\tau_{0,crit}$	=	critical shear stress
τ_{crit}	=	effective critical shear stress
Θ_{crit}	=	critical Shields number
θ_i	=	jet impact angle

REFERENCES

1. Bin AK (1993). Gas entrainment by plunging liquid jets. *Chemical Engineering Science* 48(21):3585-3630.
2. Bollaert E and Schleiss AJ (2005). Physically based model for evaluation of rock scour due to high-velocity jet impact. *Journal of Hydraulic Engineering* 131(3):153-165.
3. Brethour J (2003). TN-62 Flow Science Inc. Santa Fe. F3D Notice: Modeling Sediment Scour.
4. Chau, K.W. and Jiang, Y.W. (2001). 3D numerical model for Pearl River estuary. *Journal of Hydraulic Engineering* 127(1):72-82.
5. Chau, K.W. and Jiang, Y.W. (2004). A three-dimensional pollutant transport model in orthogonal curvilinear and sigma coordinate system for Pearl River estuary. *International Journal of Environment and Pollution* 21(2): 188-198.
6. Canepa S and Hager WH (2003). Effect of air content on plunge pool scour. *Journal of Hydraulic Engineering* 129(5):358-365.
7. De Cesare G, Daneshvari M, Federspiel M, Malquarti M, Epely-Chauvin G and Schleiss AJ (2011). Physical and numerical modeling of the spillways and plunge pools of Koman Dam in Albania. *La Houille Blanche* 3:48-55.
8. Duarte R, Bollaert E, Schleiss AJ and Pinheiro A (2012). Dynamic pressures around a confined block impacted by plunging aerated high-velocity jets. *2nd European IAHR Congress* Munich, Germany.
9. Duarte R, Bollaert E, Schleiss AJ and Pinheiro A (2014). Discussion on "CFD analysis of the effect of nozzle stand-off distance on turbulent impinging jets". *Canadian Journal of Civil Engineering* 40:603-612.
10. Federspiel MPEA (2011). *Response of an Embedded Block Impacted by High-Velocity Jets*, PhD Thesis EPFL; N 5160.
11. Flow Science Inc. (2011). *Flow-3D Help Manual - Theory*. Flow Science Flow 3D v9.3 New Mexico, USA.
12. Flow Science Inc. (2009). *Flow-3D v9.3*. New Mexico, USA.
13. Gabl R, Gems B, De Cesare G, Aufleger M (2014). Anregungen zur qualitätssicherung in der 3-D-numerischen modellierung mit flow-3D, *Wasserwirtschaft* 3(2014):20-15.
14. Gisonni C and Hager W (2008). Spur failure in river engineering. *Journal of Hydraulic Engineering* 134(2):135-145.
15. Hartung J, Elpelt B and Klösener K-H (2005). *Statistik: Lehr- und Handbuch der angewandten Statistik*, 3rd Edition, Oldenbourg Verlag, Germany.
16. Hunter TN, Peakall J, Unsworth TJ, Acun MH, Keevil G, Rice H and Biggs S (2013). The influence of system scale on impinging jet sediment erosion: observed using novel and standard measurement techniques. *Chemical Engineering research and design* 91:722-734.
17. Jenzer Althaus JMI, Schleiss AJ and De Cesare G (2011). *Sediment Evacuation from Reservoirs through Intakes by Jet Induced Flow*, PhD Thesis EPFL N 4927.
18. Kitamura JY and Wang S (2001). Simulation of scour process in plunging pool of loose bed - material. *Journal of Hydraulic Engineering* 127(3):219-229.
19. Lane EW (1955). Design of stable channels. *Transactions American Society of Civil Engineers* 120:1234-1260.
20. Laursen EM (1952). Observations on the nature of scour. *Proceedings of 5th Hydrol. Conference*, State University of Iowa, Bull., Iowa City, Iowa 34:179-197.
21. Manso P, Bollaert E and Schleiss AJ (2009). Influence of plunge pool geometry on high-velocity jet impact pressures and pressure propagation inside fissured rock media. *Journal of Hydraulic Engineering* 135(10):783-792.
22. McLean SR, Nelson JM and Wolfe SR (1994). Turbulence structure over two-dimensional bed forms: Implications for sediment transport. *Journal of Geophysical Research* 99(C6):12729-12747.
23. Ozmen-Cagatay H and Kocaman S (2011). Dam-break flow in the presence of obstacle: experiment and CFD simulation. *Engineering Applications of Computational Fluid Mechanics* 5(4): 541-552
24. Pagliara S, Amidei M and Hager WH (2008a). Hydraulics of 3D plunge pool scour. *Journal of Hydraulic Engineering* 134(9):1275-1284.
25. Pagliara S, Hager WH and Unger J (2008b). Temporal evolution in plunge pool scour. *Journal of Hydraulic Engineering* 134(11):1630-1638.
26. Pagliara S, Hager WH and, Minor H-E (2006). Hydraulics of plane plunge pool scour. *Journal of Hydraulic Engineering* 132(5):450-461.
27. Rouse H (1940). Criteria for similarity in the transportation of sediment. *Proceedings of 1st*

Hydraulic Conference, State University of Iowa, *Bull.* 20, Iowa City, Iowa, USA.
28. Schoklitsch A (1932). Ueber die energievernichtung durch walzen, *Wasserwirtschaft* 25(16/17):225-226.
29. Veronese A (1937). Erosion de fond en aval d'une décharge, *I.A.H.R. Meeting for Hydraulic Works*, Berlin, Germany.
30. Zhao Z, Fernando HJS (2007). Numerical simulation of scour around pipelines using an Euler coupled two-phase model. *Environmental Fluid Mechanics* 7:121-142.